ADVANCED OPTICAL MATERIALS
www.advopticalmat.de

Exploring the Ultralong Lifetime of Self-matrix 1,10 Phenanthroline and Boron-Based Room Temperature Phosphorescence Carbon Dots for Multiple Applications

*R. Blessy Pricilla, Pavel Urbanek, Jakub Sevcik, David Skoda, Jan Antos, Lukas Munster, Eva Domincova-Bergerova, and Ivo Kuritka**

Room temperature phosphorescence carbon dots (RTP CDs) are one of the newly investigated nanomaterials because of their remarkable optical characteristics. They are widely utilized in many versatile optoelectronic and security applications. Apart from synthesis, one of its challenging attributes is its lifetime at room temperature. Here, a straightforward and quick heating approach is presented for synthesizing self-matrix 1,10 phenanthroline and boron-based RTP CDs. 1,10 phenanthroline is utilized as an aromatic and hetero atom containing carbon precursor and boric acid is used as a passivating to stabilize the triplet excitons and prevent nonradiative deactivation. Various characterization techniques like TEM, XRD, FTIR, UV–vis, PL, and elemental analysis (ICP and CHNS) have been used to study the properties of self-matrix RTP CDs. The RTP CDs exhibited excellent blue-green emission when excited at 302 nm. Compared to the available literature, the novelty of this work is observed from its high naked eye phosphorescence characteristic of ≈22 s with an average lifetime of ≈ 2.4 s at 302 nm, making them ultralong self-matrix RTP CD material. Due to their exceptional qualities, the self-matrix RTP CDs have been widely employed for various applications, including information encryption decryption, phosphor for LEDs, anticounterfeiting, and water sensitivity analysis.

1. Introduction

Owing to the prospective optical applications, it is crucial to develop luminous materials with fascinating light-emitting characteristics. Room temperature phosphorescence (RTP) materials occupy a prominent position among them. RTP is a phenomenon where longer relaxation of the electrons is observed from the triplet state to the ground state.[1] The electrons capture the energy from the incident light and gradually release them as they go from the singlet to the triplet and finally to the ground state. RTP materials have captured the scientific community's attention because of their prolonged lifetimes and Stokes shift. Their hallmark of longer lifetimes makes them exclusively used in applications like bioimaging,[2] sensors,[3] information encryption,[4] anticounterfeiting etc.[5] Various synthesis methods to obtain RTP materials include heating,[6] hydrothermal and,[7] microwave.[8] Notably, synthesizing RTP materials at ambient conditions is quite challenging because of the weak spin-orbit coupling effect and quenching of triplet excitons.[9] Nevertheless, some of the key mechanisms responsible for achieving effective intersystem crossing and enhancing spin-orbit coupling include lone pair electron incorporation, heavy atom effect, Hyperfine coupling, energy gap narrowing, molecular aggregation, host guest complexation, matrix rigidification, polymerization, crosslinking, and clusterization.[10] The conventional RTP materials include noble metal compounds,[11] pure organic compounds, and[12] compounds containing rare earth elements.[13] However, they suffer from several limitations like high cost, difficult synthesis, high toxicity, and shorter lifetime and luminescence.[14] Hence, the quest to search for alternative materials continues.

Among the many phosphor materials, carbon dots (CDs) have begun to take the role of RTP materials because of their high carbon content leading to less potential toxicity, simple synthesis, and tunable photoluminescent characteristics.[15] CDs are zero-dimensional nanomaterials discovered in the year 2004.[16] The phosphorescence characteristics of CDs mainly originate from n-π^* transitions, surface functional groups, and subflurophores.[17] There are two ways to achieve RTP of CDs namely matrix-free, and,[18] Matrix-dependent.[19] Matrix-free or self-matrix RTP CDs are created in a single step where the synthetic medium or the side products can be created concurrently while the emissive CDs are created at high temperatures. Matrix-dependent RTP CDs involve a two-step synthesis. In the first step, the CDs are synthesized and the second step involves the embedding of the guest

R. B. Pricilla, P. Urbanek, J. Sevcik, D. Skoda, J. Antos, L. Munster, E. Domincova-Bergerova, I. Kuritka
Centre of Polymer Systems
Tomas Bata University in Zlin
Tr. T. Bati 5678, Zlin 76001, Czech Republic
E-mail: kuritka@utb.cz

The ORCID identification number(s) for the author(s) of this article can be found under https://doi.org/10.1002/adom.202400753

DOI: 10.1002/adom.202400753

CDs into the host matrix. Some of the commonly used matrixes include PVA,[20] polyacrylamide,[21] urea,[22] silica,[23] melamine and,[24] boric acid.[25] Among the two categories, self-matrix RTP CDs are more preferred as it is more simplified and faster. Despite its simplicity, some challenges are followed. Some of the main challenges faced for this demanding synthesis include instability of excited triplet species, oxygen-induced phosphorescence quenching, and inefficient intersystem crossing.[26] Hence, to meet these challenges, a good RTP material should include efficient intersystem crossing from the lowest singlet state to the ground state, faster phosphorescent decay from the lowest triplet state to the ground state, and reduction of non-radiative decay and quenching processes.

Keeping all these factors in mind, we have synthesized self-matrix ultralong RTP CDs using Boric acid and a carbon source compound through the well-known heating method.[27] Here, 1,10 phenanthroline was used as a precursor for self-matrix RTP CDs. The reaction was carried out for several hours at a relatively mild temperature of 200 °C. This method is simple, inexpensive, non-toxic and highly efficient in obtaining stable material containing self-matrix RTP CDs in gram scale. Moreover, 1,10 phenanthroline has the potential to provide carbon as well as nitrogen source. The presence of hetero atom and aromatic conjugated system provides suitable structural motifs for incorporating into self-matrix RTP CDs and increases the spin-orbit coupling. This leads to efficient intersystem crossing, thus making it a good candidate as a source material with great potential to obtain ultralong self-matrix RTP CDs. It was verified that there is no emission attributable to residual 1,10 phenanthroline in the material. Boric acid is structurally simple and stable. Generally, metaboric or pyroboric acid is expected as a product of its dehydration when heated. Its electron-accepting feature and empty p orbital make it potentially a good candidate to be used in RTP materials.[28] The n-π^* transitions and the B-C covalent bonding in the synthesized self-matrix RTP CDs play an effective role in the ultralong RTP of the CDs obtained. Even though some self-matrix RTP CDs have already been reported, our work stands out from the literature because of addressing the challenge of self-matrix RTP lifetime. The novelty of the work has been demonstrated by selecting suitable precursors to observe an outstanding naked eye phosphorescence of ≈22 s under 302 nm. The average lifetime was found to be 2.4 s, which is a highly competitive value in the literature to be achieved. The exceptional RTP properties of the synthesized CDs have effectively been utilized in various applications such as digital encryption, anticounterfeiting, phosphor for LED, and fingerprint detection.

2. Results and Discussion

2.1. Synthesis and Characterizations of Self-Matrix RTP CDs

Using a heating method, the self-matrix RTP CDs were created in a condensed phase from an aqueous solution comprising boric acid and 1, 10 phenanthroline.[27] The obtained product had a glassy state emitting blue fluorescence when excited at 302 nm. However, after the UV Light is turned off, cyan phosphorescence is observed. The extraordinary naked eye phosphorescence of ≈22 s at 302 nm of the self-matrix RTP CDs indicates their ultralong phosphorescence performance. The schematic illustration of the synthesis of self-matrix RTP CDs is shown in **Scheme 1**.

The morphological studies of the self-matrix RTP CDs was carried out using TEM. The individual dots and aggregates of the dots are visible in the TEM image in **Figure 1a**. The average particle size as calculated from ImageJ software was ≈9.6 nm. The Particle size distribution of the RTP CDs has been represented in the form of a histogram in Figure 1b. The polycrystalline nature of the self-matrix RTP CDs material can be seen in the XRD spectra in Figure 1c. The overall shape of the diffractogram and the intense broad background are signs of the prevailing glassy state of the material. For comparison, the XRD diffractograms of the pure Boric acid and 1, 10 phenanthroline have been presented. The diffractograms of the blank sample (boric acid with water additon but without 1,10 phenantroline, heated and cooled under the same conditions as the sample) and self-matrix RTP CDs can be compared in the graph in the supplement (Figure S3, Supporting Information). The heated boric acid was observed to have similar peak positions as RTP CDs. However, the peak at 28° is observed to have a minor split as shown in Figure S3 (Supporting Information) (28.1° and 28.3°). The three dominant peaks of the self-matrix RTP CDs are observed at 28.1°, 14.8°, and 43.1°. These peak positions are similar to those of prominent peaks observed in boric acid, metaboric acid, and boron trioxide whereas no pyroboric acid data were available in the database. Therefore, no unambiguous attribution to the available pdf cards was possible to the self-matrix RTP CDs diffractogram. The broadness of the peaks implies nanosize of coherently diffracting domains; however, without a knowledge of how many peaks are eventually merged in one broad line, precise analysis is also excluded. Predominantly, the peak at 28° indicates the triclinic phase. On the other hand, the splitting of this peak observable in the blank sample, see the inset in the diffractogram (Figure S3, Supporting Information), indicates the presence of two but very similar phases, but even then, they are not distinguishable. The sharp peaks observed in 1,10 phenanthroline, or any other peak attributable to this compound or its degradation products, if present, are concealed in the XRD pattern of self-matrix RTP CDs due to the low loading amount of 1,10 phenanthroline comparatively.[29]

The mass loss was calculated to understand the structure of our final product. The product yield of the self-matrix RTP CDs was 1.72 g, and a mass loss of 1.29 g was observed compared to the initial concentration. This represents a relative loss of ≈42% of the initial sample mass. Theoretically, a relative weight loss of 29%, 36%, and 43.7% can be attributed to the formation of metaboric acid, pyroboric (also known as tetraboric) acid, and boron trioxide (due to water release from orthoboric source compound). The boric acid decomposition is known in the literature.[30,31] We compared the thermal decomposition of boric acid under dry and wet synthesis conditions using the same concentration of the starting precursor. Amounts of 3 g of boric acid were weighed into two separate beakers individually. The first beaker was heated with only Boric acid and the second beaker was heated by adding 40 mL of water. The heating and cooling conditions were the same as the synthesis conditions for self-matrix RTP CDs. In the first beaker containing dry boric acid, a mass loss of 1.083 g was observed corresponding to a relative mass loss of 36.1% indicating the formation of pyroboric acid. In the second beaker, the mass loss was 1.207 g, corresponding to a

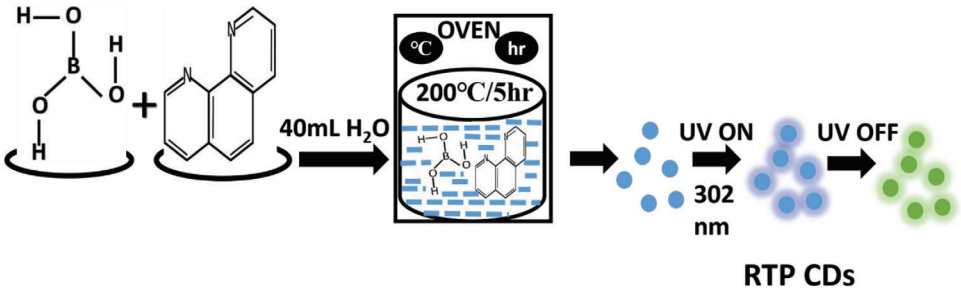

Scheme 1. Schematic representation of the synthesis of self-matrix RTP CDs.

relative mass loss of 40.2%, indicating a blend of pyroboric acid and boron trioxide. The incomplete transformation to well-defined dehydrated compounds and blended character of the product is in accordance with the ambiguous character of obtained XRD patterns. Unlike the dry pathway, it seems the presence of water or humid conditions enhances the decomposition of boric acid to boron trioxide, although less than 100% conversion was observed. Alternatively, the addition of water might have enhanced the sublimation of ortho- and metaboric acids, but no deposits outside the beaker were observed. According to the literature, the heating mode and vapor pressure play an important role in the drying, sublimation, and dehydration processes of boric acid.[32]

Elemental analysis was performed to estimate boron, carbon, oxygen, and hydrogen content in the prepared self-matrix RTP CDs material. ICP analysis revealed the mass concentration of boron (24.5 ± 0.2%) in the material which corresponds to metaboric acid with a theoretical boron content of 24.7%. CHNS

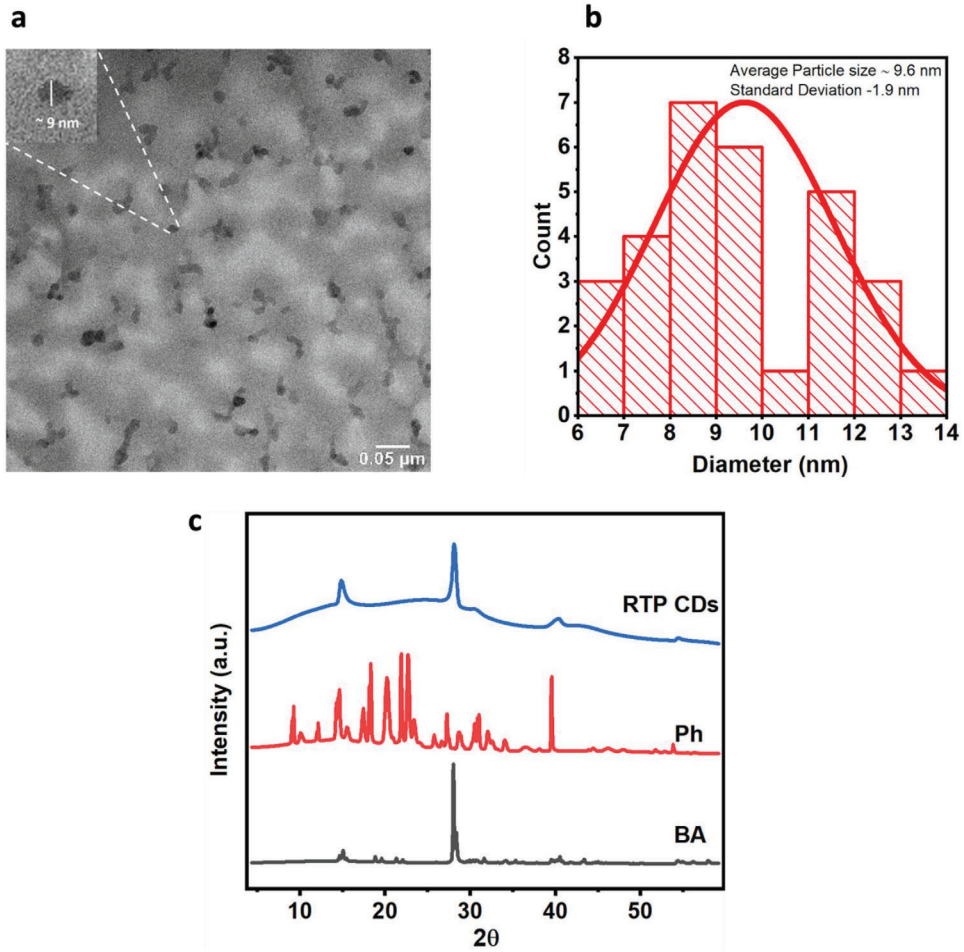

Figure 1. a) TEM image of self-matrix RTP CDs b) Particle size distribution of RTP CDs c)XRD spectra of Boric acid (BA), 1, 10 phenanthroline (Ph) and Self-matrix RTP CDs.

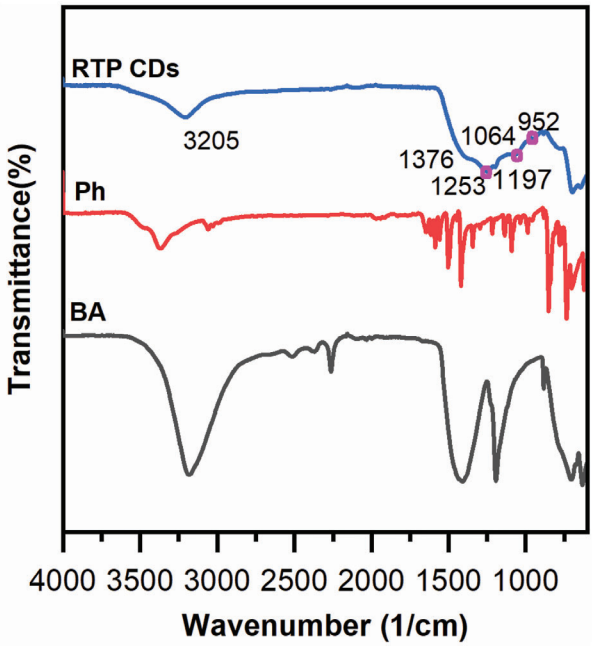

Figure 2. FTIR spectra of Boric acid (BA), 1, 10 phenanthroline (Ph), and Self-matrix RTP CDs.

analysis revealed no presence of sulfur, and mass concentration of nitrogen ≈0.5%, carbon 0.4%, and 2.75% of hydrogen. The values of 0.5% are close to the limit of detection for this method indicating thus minute amounts of these elements present in the material which corresponds to the initial composition of the reaction mixture. The concentration of hydrogen corresponds closely to the metaboric acid formula. On the other hand, humidity is an irreplaceable contaminant in our synthesis condition.

We examined the self-matrix RTP CDs using Fourier Transform Infrared spectroscopy (FTIR) to understand their composition. For a better understanding of the self-matrix RTP CDs, the FTIR spectra of the precursors were also compared.

As can be seen in **Figure 2**, the characteristic peaks of Boric acid and 1, 10 phenanthroline can be clearly observed in their respective spectra.[33,34] However, due to the very low loading content of the organic precursor, it cannot be expected that more than 0.5% of the carbonaceous compound is present in the self-matrix RTP CDs material. Hence, the peaks attributable to carbonaceous species are hardly visible in the spectrum. The peak observed at 3205 cm^{-1} in self-matrix RTP CDs is attributed to the O—H functional group. This group promotes the formation of hydrogen bonds which ultimately help in stabilizing the triplet excited states. Absorption bands corresponding to vibrational modes of B—O—H and B—O—B structural moieties are expected in the region ≈from 1570 to ≈900 cm^{-1}. Nevertheless, a merged broad band is observed for self-matrix RTP CDs material instead of separated peaks as observed for boric acid in the spectrum. This can be attributed to the glassy state of the material and depreciation of the B—OH corresponding signal due to dehydration of the starting material. The peak observed at 1376 cm^{-1} superposed on the shoulder of the broadband can be attributed to COO^- symmetric stretching.[35] The peak found at 1197 cm^{-1} is because of the stretching B-O—H vibrations.[36] Three distinct peaks were ascertained only in self-matrix RTP CDs. The new peak observed at 1253 cm^{-1} indicates the formation of a B-C bond suggesting the blending of boric acid into the structure of 1,10 phenanthroline.[37] The unique broad shoulder peak at 1064 cm^{-1} is most likely due to the C-O/C-N stretching vibrations. The weak band observed at 952 cm^{-1} implies symmetric stretching of the B—O bond in BO_3 and/or BO_4 units.[38] The other minor peaks observed in self-matrix RTP CDs are similar to the peaks observed in boric acid with slight shifts in the peak positions.

According to the literature, XPS is a powerful tool for analysis of the composition and chemical states of the elements built in the prepared CDs.[38,39] Nevertheless, this requires isolation of the CDs whereas measurement on the self-matrix RTP CDs material can be disputable. An example of a straightforward analysis is available in the literature.[6] In our case it was demonstrated that surface contamination by adventitious carbon ascertains up to tens of percent and overlays any signal of the carbonaceous component in the self-matrix RTP CDs, where the concentration of carbon in the form of CDs can be expected 0.5% or lower. Thus, the analysis of C1s high-resolution spectra lacks useful information. Similarly, the spectra for B1s and O1s do not reveal specific information for the dots, confirming just a presence of the boric acid-derived matrix. Only the N1s spectrum fitted by two subpeaks at 399.9 eV and 402.11 eV are suggestive of the presence of C═N—H and N—H bonds, respectively (Figure S4, Supporting Information).[40,41]

To summarize the structural and compositional analysis of the self-matrix RTP CDs material nature, a mixture consisting of HBO_2 and B_2O_3 is most likely obtained as the matrix under given conditions. The mixture is a viscous fluid at an elevated temperature and transforms into a glassy state when cooled and obtained. If the product is regarded as a hydrate of boron oxide, it can be formulated as $B_2O_3 \cdot xH_2O$ (where $x \leq 1$) in which self-matrix RTP CDs are dispersed in a mass concentration of 0.5% or less.

2.2. Optical Properties

The UV reflectance spectrum helps in understanding the electronic configuration of the synthesized self-matrix RTP CDs. The UV spectrum in **Figure 3** shows three prominent absorption peaks for self-matrix RTP CDs material and almost no absorption was observed for the blank sample containing only the product without any phenantroline-derived component. The blank sample behaves as a nearly white standard. The occurrence of the peak at 233 nm is due to π-π^* transition of of C═C band.[42] At 280 nm, the electronic transition of π-π^* of the conjugated C═N bond is observed.[43] To this electron transition band, the C = O n-π^* transitions can contribute. Moreover, at 320 nm n-π^* electronic transition of CN = bond is noted here.[43] Spin orbit coupling is enhanced by the presence of such groups like C═N/C═O. As a result, efficient intersystem crossing, and triplet generation is attained.[44] There is also a shoulder peak at ≈360 nm indicating a specific absorption. The absorption edge starts at ≈380 nm. For comparison, 1,10 phenanthroline has absorption maxima at 232 and 264 nm in CH_2Cl_2 solution at room temperature according to the literature.[45]

The PL characteristics of 1, 10 phenanthroline was studied to understand its characteristic feature. The emission of 1,10

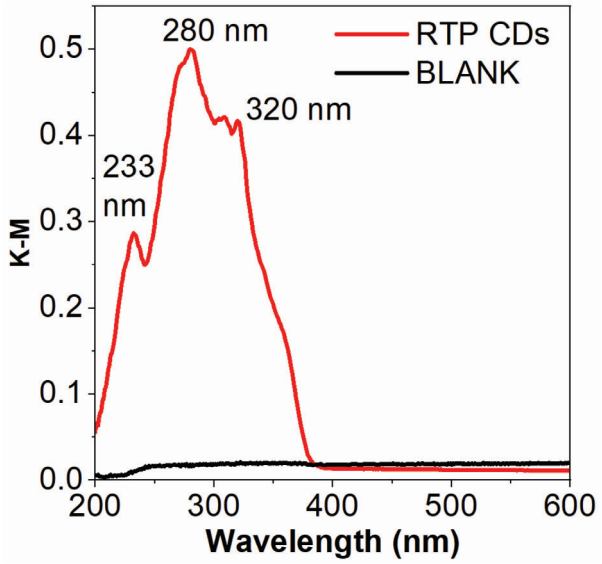

Figure 3. UV–vis spectra of seůf matrix self-matrix RTP CDs.

phenanthroline in UV mainly originates from radiative deexcitation of π-π* singlet excited states whereas a weak fluorescence with vanishingly low emission quantum yield is observed due to n-π* transitions which allow non radiative transitions. It has a fluorescence with emission maxima at 358 nm and 376 nm in CH_2Cl_2 solution at room temperature while no phosphorescence is observed. Nevertheless, it has a phosphorescence at liquid nitrogen temperature (77 K) with emission maxima at ≈460, 490, and 525 nm.[45] Therefore, control experiments were conducted to understand the luminescence characteristics of self-matrix RTP CDs and to exclude the effects of residual starting components in the self-matrix RTP CDs as 1,10 phenanthroline is a known luminescent compound. For such confirmation, an experiment was conducted where pure compounds and mixtures of 1,10 phenanthroline and BA were prepared and the photoluminescence properties of these materials were studied. 1, 10 phenantroline was embedded by mixing into the BA matrix, and its PL characteristics were studied in dry and wet form (Figure S1, Supporting Information). As can be seen, 1,10 phenanthroline is a fluorophore with no RTP. Nevertheless, it keeps its characteristic fluorescence emission observed in all samples with prominent peaks at ≈365 nm and an additional peak at 378 nm in the long wavelength shoulder.

Furthermore, the fluorescence and phosphorescence of self-matrix RTP CDs have been investigated in detail. Initially, when the excitation source, UV light is on, a bright blue emission is observed. A long-lifetime emission of cyan color is observed when the UV light is switched off. To understand the phosphorescence characteristics of the self-matrix RTP CDs, a specific setup as described in the experimental section was used. The Photoluminescence spectra of self-matrix RTP CDs excited at 302 nm is shown in **Figure** 4a. The results from the verification experiment allow us to claim that no 1,10 phenanthroline emission is present confirming its total conversion during the material synthesis. The envelope of the PL spectra (Figure S1c, Supporting Information) shows both fluorescence and phosphorescence peaks including a small contribution due to the scattered excitation light from the UV lamp. The fluorescence and phosphorescence peaks in Figure 4a have been deduced from the envelope of the PL spectra. For better understanding a 3D graph showing the complete PL spectra with respect to time has been shown in Figure 4b,c. As can be observed, when the excitation source is on, all three peaks are observed clearly. However, when the excitation source is off the the peak at around 300 and 400 nm disappears immediately and the peak centered ≈471 nm gradually decreases with time. As a result, it may be concluded that the peaks seen at roughly 400 and 471 nm correspond to fluorescence and phosphorescence, respectively. The shoulder peak of phosphorescence around 530 nm might be due to the vibrational energy levels of the primary phosphorescence peak or due to the vibrations of the aromatic system.[46,47] The RTP CDs at 302 nm were found to have a significant total quantum efficiency of 33%. The fluorescence and phosphorescence quantum yield was found to be 9% and 24% respectively. The CIE coordinates of self-matrix RTP CDs were calculated to demonstrate the PL and phosphorescence color emission. The obtained PL and phosphorescence emission color coordinates as shown in Figure 4d are (0.18, 0.22) and (0.19, 0.31) respectively.

An excitation-emission map (Figure S2, Supporting Information) was investigated to understand the behavior of self-matrix RTP CDs with respect to the excitation wavelength. The emission map is shown from excitation wavelength 250 to 370 nm (Figure S2b, Supporting Information). The maximum emission of ≈400 and 477 nm was observed for an excitation wavelength of 360 nm. It was observed that the fluorescence peak around 400 nm remains constant, independent of the excitation wavelength. The main phosphorescence peak observed at ≈477 nm was found to have some dependency on the excitation wavelength as the emission peaks slightly varied by few nanometres with respect to the excitation wavelength. The minor phosphorescence shoulder peaks at ≈447 and 500 nm are due to the vibrational transitions occurring between the various energy levels of the singlet and the triplet states. The excitation spectra corresponding to the fluorescence emission maximum and the phosphorescence maximums have been demonstrated (Figure S2a, Supporting Information). It is also important to note that the phosphorescence of self-matrix RTP CDs is quenched in water as illustrated in the application in Figure 8. Compared to excitation dependent emission spectrum in CDs excitation independent emission spectrum is less common to observe. In our case, we have obtained excitation independent strong blue fluorescence emission spectrum at 400 nm as can be seen Figure 4a (Figure S2b, Supporting Information). A simple core structure and uniform surface state aid toward obtaining excitation independent PL emission spectrum. The non shifting emission spectra of CDs could also be as a result of fewer surface states comparatively or their passivation. The surface states of the CDs can be also blocked due to embedding in a rigid matrix.[48–50] The excitation independence of the PL and its single exponential decay testify to a well-developed simple core structure. The low number or passivation of surface states is also proved in the FTIR spectra of self-matrix RTP CDs which are poor of absorption bands associated with carbonyl, ester, and amide groups (Figure 2).

The optical properties of the self-matrix RTP CDs were also investigated by varying the precursor ratios and the synthesis conditions within the preliminary heuristics aiming at the best

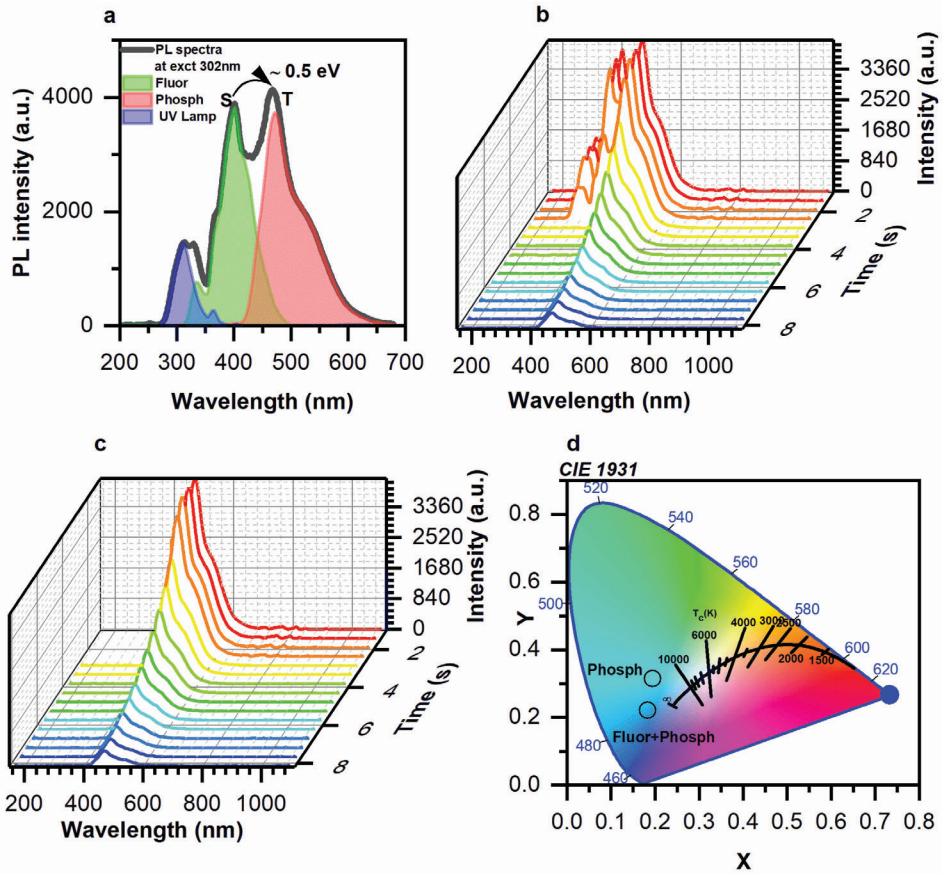

Figure 4. a) Fluorescence (Fluor) and phosphorescence (Phosph) spectra of self-matrix RTP CDs along with the emissionof the UV lamp (302 nm) b) Fluorescence and phosphorescence spectra of self-matrix RTP CDs with respect to time (λ_{exct} = 302 nm) c) Phosphorescence spectra of self-matrix RTP CDs with respect to time (λ_{exct} = 302 nm) d) Chromaticity diagram showing the color coordinates of self-matrix RTP CDs (Fluor +Phosph) and their phosphorescence (Phosph) respectively.

performing material. The effect of these parameters on the phosphorescence lifetime of self-matrix RTP CDs was studied. The precursor ratios were investigated by varying the amount of 1,10 phenantroline in the boric acid-based matrix. The concentration of Boric acid was kept constant (3 g) and the concentration of 1,10 phenanthroline (10, 20, 50, and 100 mg) was varied. It was observed that with an increase in the concentration of 1,10 phenanthroline in the BA matrix, the average lifetime of self-matrix RTP CDs is found to be decreasing (Table S1, Supporting Information). Probably, the increase in the precursor concentration disrupted the rigidity of the BA matrix.[51] Consequently, a concentration of 10 mg of 1,10 phenanthroline was selected as the optimal concentration for all investigations. **Figure 5**a,b shows the average lifetime of fluorescence and phosphorescence of self-matrix RTP CDs. A single exponential decay fit was used to find the average fluorescence and phosphorescent decay. The average fluorescence and phosphorescence lifetime was found to be 7.51 ns and 2.4 s respectively when excited at 332 and 302 nm. Figure 5c shows the 22 s naked eye phosphorescence lifetime of self-matrix RTP CDs with time. The supplementary information shows the video of the observed naked-eye phosphorescence of the self-matrix RTP CDs.

The effect of temperature as the main synthesis parameter was also investigated on the phosphorescence lifetime which is the main material property. The various lifetimes obtained on samples prepared at temperatures 180, 200, 220, and 240 °C are depicted (Table S2, Supporting Information). It was observed that the glassy state of the self-matrix RTP CDs was formed only above 180 °C. Since for effective entrapment of the electrons in the glassy state 180 °C is considered important, hence the temperatures above 180 °C were chosen for the study purpose. It was noted that only a few milliseconds difference exists between 200 and 220 °C. We tested synthesis temperatures up to 240 °C. At this temperature, the phosphorescence lifetime was reduced to a value of ≈2 s. Consequently, the temperature of 200 °C was selected as the best temperature condition for the synthesis of self-matrix RTP CDs. This high average phosphorescence lifetime of ≈2.4 s with naked eye phosphorescence of ≈22 s is very rare to find in self-matrix RTP CDs. The available literature has been compared to this work, and the results are demonstrated. (Table S3, Supporting Information).

2.3. Mechanism of RTP

Based on the obtained results, the following mechanism has been predicted for the RTP of the CDs (**Scheme 2**). A Jablonski diagram has been demonstrated for a better understanding.

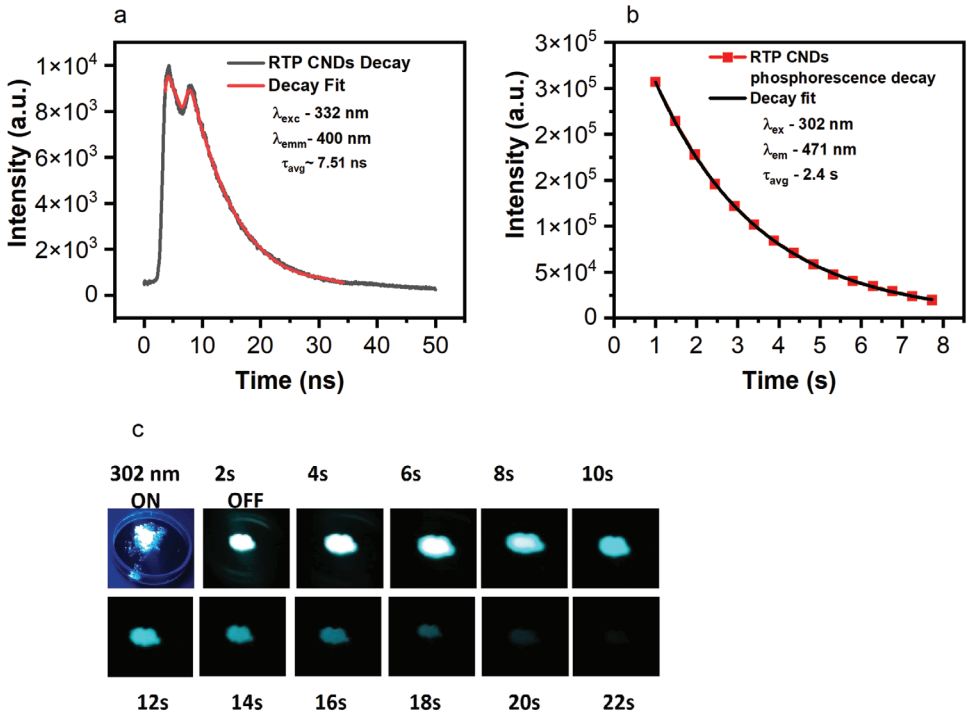

Figure 5. a) Fluorescence and b) An Example of phosphorescence time decay response curve of self-matrix RTP CDs (c) Naked eye phosphorescence of self-matrix RTP CDs.

Generally, when the light is irradiated on the CDs, the electrons in the ground state (S_0) get excited to singlet excited states (S_1-S_n). The scheme based on the graph in Figure 4a shows that the material follows the standard pathway known from the literature.[52] The singlet excited states either go through internal conversion and go to the ground state, emitting fluorescence with a maximum at the wavelength of 400 nm, or experience intersystem crossing to triplet excited states and go to the ground state, leading to phosphorescence with a maximum at the wavelength above 470 nm.

To observe phosphorescence some of the key factors involve the use of hetero atoms and aromatic carbonyl groups. These tend to increase the spin-orbit coupling which finally leads to efficient intersystem crossing. In our work, the selection of the organic precursor was based on the nitrogen heterocycle strategy to obtain effective intersystem crossing leading to outstanding RTP. The introduction of Boron atoms into the aromatic and hetero atom containing 1,10 phenanthroline expedites the transition of singlet excitons to triplet states by lowering the energy gap between the singlet and triplet state.[36] The bandgap energy values

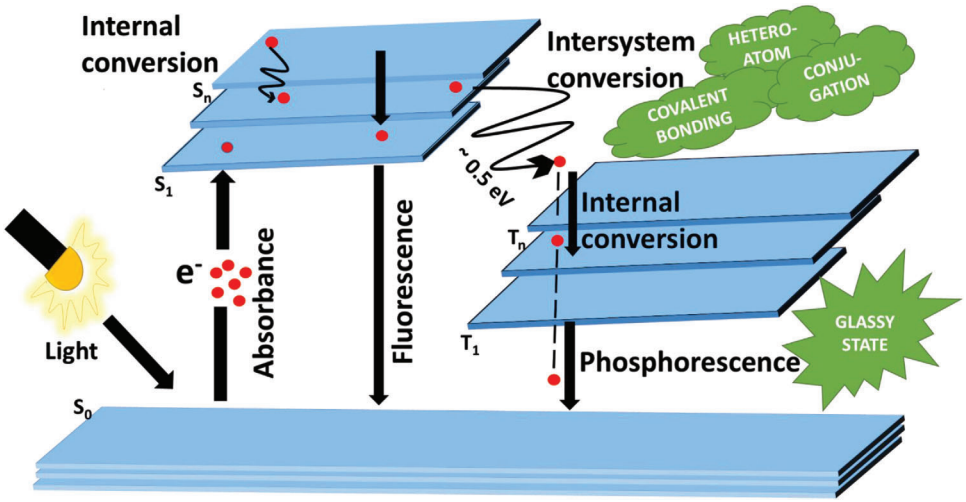

Scheme 2. Schematic representation of the mechanism of self-matrix RTP CDs.

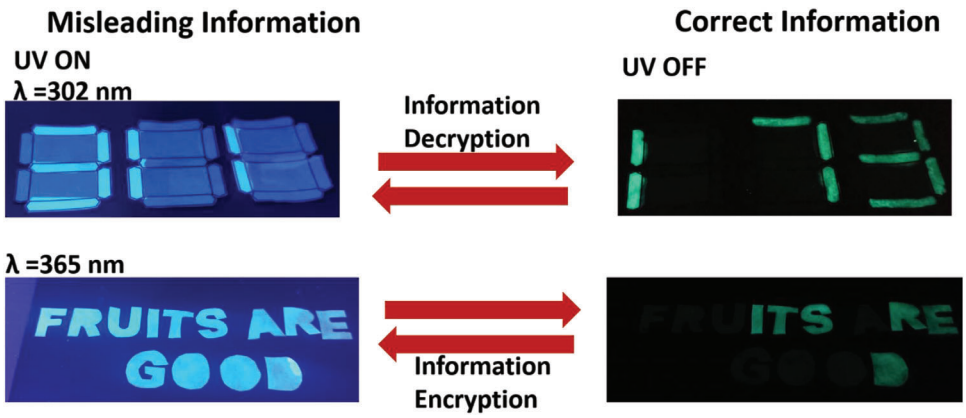

Figure 6. Information encryption decryption representation using self-matrix RTP CDs.

of the singlet (E_{S1}) and triplet state (E_{T1}) were calculated using the following Equation (1):

$$E\ (eV) = 1240 / \lambda \quad (1)$$

The calculated energy values of E_{S1} and E_{T1} are 3.1 and 2.6 eV, corresponding to the emission maxima wavelengths at 400 and 477 nm. The difference in these energies provides the energy bandgap (ΔE_{ST}) between the singlet and triplet states. The calculated ΔE_{ST} value is 0.5 eV. This value is small thus allowing for effective Intersystem crossing. The presence of C═N bonds greatly enhances the triplet emission. During the heat treatment, a rigid network of new covalent bonds B—O—B is established in the process of boric acid condensation including a possibility of B-C bond formation. Such bonding arrangement in the nearest proximity of the CDs' surface plays an effective role in stabilizing the overall system leading to effective RTP emission. Boron atoms in the glassy matrix can enter p-π conjugation. A vacant p orbital effectively attracts π electrons of adjacent conjugated aromatic systems and leads to reduced free orbital energy levels. The glassy state of the self-matrix plays an important role in obtaining adequate RTP of CDs. It prevents the triplet excitons from undergoing nonradiative emission. By restricting the vibrations and rotations of the functional groups, it leads to increased radiative transition of triplet excitons.[36] The matrix confinement also prevents aggregation-induced quenching in the solid state, thus promoting RTP,[53] although examples of aggregation-induced emission were also reported.[54] Moreover, the presence of functional groups like C—N, O—H, C—N, B—O, and NH_2 greatly enhances the RTP by forming hydrogen bonds and stabilizing the triplet species.[55]

2.4. Applications

Owing to the excellent phosphorescent properties of the self-matrix RTP CDs, they have a great potential to be effectively employed in various applications like information protection, data encryption, anticounterfeit, and fingerprint detection. To substantiate these applications, the potential of self-matrix RTP CDs was demonstrated. First, self-matrix RTP CDs were used as a security ink on a filter paper. For the purpose of fake ink, salicylic acid in ethanol was used. The use of self-matrix RTP CDs as security ink for information protection is shown in **Figure 6**. The required template was printed on the filter paper. The fake ink was painted to write the misleading information and the self-matrix RTP CDs were used to write the correct information on the filter paper. When the filter paper was irradiated with a UV lamp of 302 nm, the fake information "3 1 1" was visible. However, due to the excellent phosphorescence characteristics of self-matrix RTP CDs the correct information "1 7 3" was visible after the removal of the UV lamp. Thus, verifying the application of the self-matrix RTP CDs as security ink for information protection. Another demonstration for data encryption is shown in Figure 6 (bottom) where the misleading information "FRUITS ARE GOOD" is observed under UV lamp irradiation of 365 nm, but as soon as the irradiation is removed the secret correct information "ITS RED" is decrypted.

Second, the anticounterfeit application of the self-matrix RTP CDs has been demonstrated. As can be seen in **Figure 7a**, two types of scan codes were created based on our university websites. The scan code on the left contains the correct information however, the scan code on the right depicts the wrong information. The left scan code with the correct information has been painted with self-matrix RTP CDs ink and dried. Under the UV light of 302 nm, both the scan codes appear blue however when the light is switched off, the correct information on the left is seen showcasing the green light while the code on the right side with the wrong information disappears.

Thirdly, the use of self-matrix RTPCDs for fingerprint detection has been illustrated. Fingerprint detection plays a key role in the identification of a person.[56] Most often, due to poor optical contrast of the background, fingerprint detection becomes difficult. Hence, it is suggested to use phosphorescent materials which overcome the challenge of contrasting backgrounds and provide clear information about the different parts of a fingerprint. Some of the examples of the methods used to identify fingerprints include powder dusting, iodine fuming, silver nitrate development etc. Among the many, the powder dusting method was used because of its simplicity and cost-effectiveness. In our work, we used this method to obtain the fingerprints. According to this method, the mechanical adhesion of the powder to the oily parts of the fingerprint deposits is used to obtain the fingerprints on the substrates.[57] The self-matrix RTP CDs were able

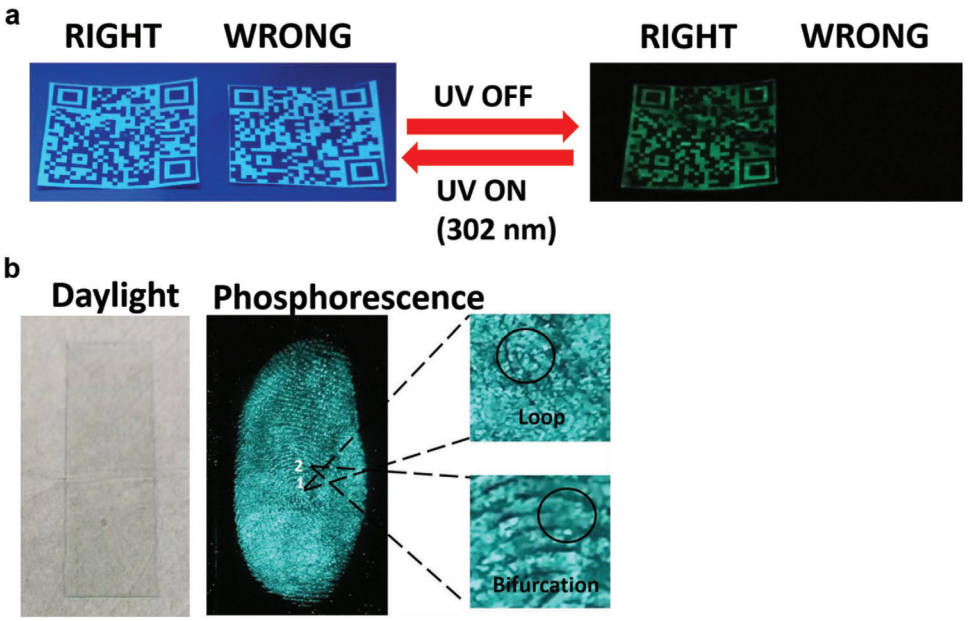

Figure 7. a) anticounterfeit application of self-matrix RTP CDs b) Fingerprint detection using self-matrix RTP CDs.

to effectively adhere to the fingerprint that was obtained on the glass substrate. As can be seen in Figure 7b, under daylight the fingerprint can't be observed with the naked eye. After equally spreading the self-matrix RTP CDs all over the fingerprint, the phosphorescence images are obtained after excitation of 302 nm. It is also noteworthy that different parts of the fingerprint like bifurcation and loop can also be observed. Hence, we suggest the use of self-matrix RTP CDs as an effective phosphor material for fingerprint detection.

Fourthly, we demonstrate the use of self-matrix RTP CDs in the stimuli responsive class of materials. The water sensitivity of self-matrix RTP CDs was used for sensing applications. In **Figure 8**, self-matrix RTP CDs on the left are wet and the right side self-matrix RTP CDs are dry. It was observed that after the UV excitation of 302 nm was switched off, the phosphorescence of the wet CDs was quenched within a few seconds. This is mainly due to disturbance caused to the rigid BA matrix by the H_2O moieties. In a solid state, the vibrational and rotational movement of the emitting groups is restricted, leading to slow and effective phosphorescence. However, the movements of the emitting groups are set free in an aqueous state leading to possible non-radiative recombinations.

Finally, the self-matrix RTP CDs were employed as a phosphor material for LED applications because of their excellent optical capabilities. Free-standing self-matrix RTP CDs thin films of ≈450 µm were fabricated using a press with an applied pressure of 50 kN. These films were placed on top of 310 and 340 nm LEDs to serve as phosphors converting the UV excitation into a visible light emission and their characteristics were recorded.

As can be seen from the emission spectra in **Figure 9a**, the UV excitation light from exciting diodes has been absorbed by self-matrix RTP CDs and only visible light is produced. The luminance of such devices (excitation LED/450 µm thick self-matrix RTP CDs layer) was 55 cd/m^2 for both excitation wavelengths of the diodes. It should be noted, that this luminance value can further be optimized for better performance. The chromaticity diagram in Figure 9b indicates the color of the devices. The CIE x,y coordinates of the 310 nm driven device are 0.186, 0.227 and the 340 nm driven device are 0.184, 0.231. Hence, these self-matrix

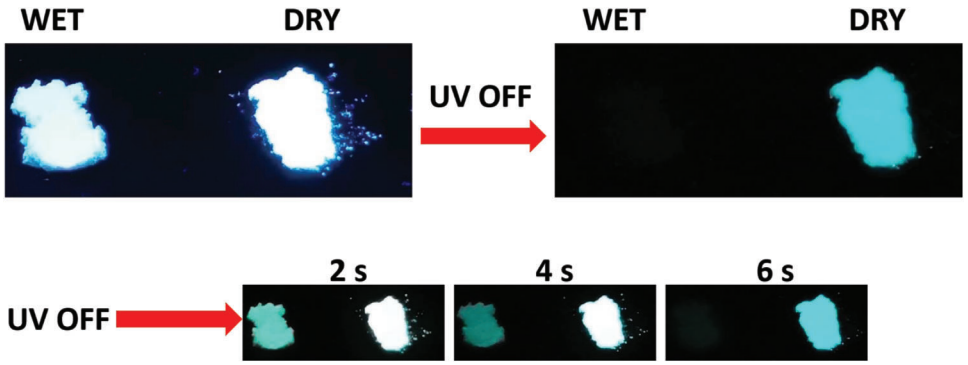

Figure 8. Sensitivity of self-matrix RTP CDs toward water.

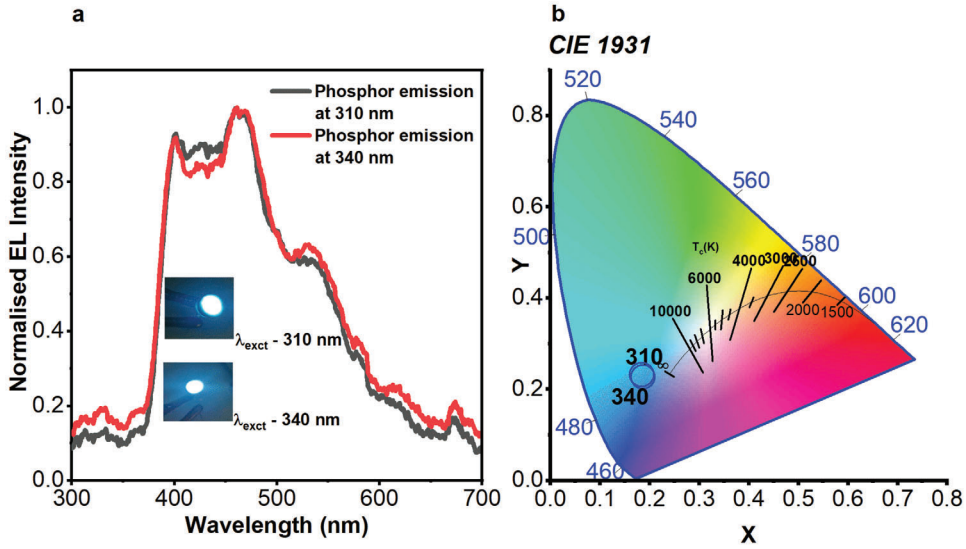

Figure 9. a) EL spectra of self-matrix RTP CDs on LED diodes 310 and 340 nm b) Chromaticity diagram showing the color coordinates of self-matrix RTP CDs on LED diodes 310 and 340 nm.

RTP CDs showcase a high potential to be used as a phosphor for blue light source driven by UV LEDs. The complete absorption of the UV light which was observed offers also a possibility to use the self-matrix RTP CDs as a material for the construction of UV filters.

3. Conclusion

In summary, the heating method was used for the successful synthesis of self-matrix RTP CDs. It is a very simple method involving the entrapment of 1, 10 phenanthroline in the matrix of boric acid using a simple heat treatment approach leading to the formation of ultralong self-matrix RTP CDs. The resulting self-matrix RTP CDs have superior structural, optical and functional characteristics. They exhibit excellent solid-state phosphorescence characteristics by providing 22 s naked eye phosphorescence when excited at 302 nm. Compared to the self-matrix RTP CDs in the literature, its appealing 2.4 s average lifetime makes it highly competitive. The rigidity of the self-matrix obtained restricts the vibrational and translational movements leading to effective RTP. The highly efficient self-matrix RTP CDs have been utilized for a variety of applications like information encryption decryption, anti-counterfeiting, sensing, fingerprint detection, and as an effective LED phosphor material. This study on solid-state self-matrix RTP CDs, paved the way to produce self-matrix CDs with outstanding phosphorescence characteristics utilizing economical precursors for versatile applications.

4. Experimental Section

Materials: Boric acid and 1,10 phenanthroline were bought from Sigma Aldrich. The UV LED diodes were acquired from Roithner Lasertechnik, Austria. All the chemicals were used without any further purification. The conductivity of the water used was 0.09 μS cm^{-1} with a 6.3 pH.

Characterization: The morphological study was carried out on the TEM model, JEOL JEM 2100 microscope, operated at 300 kV (LaB6 cathode, point resolution 2.3 Å equipped with OLYMPUS SYS TENGRA camera (2048 × 2048 pixels)). The self-matrix RTP CDs were dispersed in water and a few drops were coated on the TEM grid. The grid was dried overnight and imaging was carried out. ImageJ software was used to analyze the particle size. Powder XRD patterns were attained on an X-Ray powder diffractometer (Rigaku Miniflex 600) using Co Kα radiation (λ = 1.7903 Å), operated at a beam voltage of 40 kV and a beam current of 100 mA. PowDLL Converter was used to convert Co Kα radiation to Cu Kα radiation (λ = 1.54 Å). The Fourier Transform Infrared (FTIR) spectra analysis was obtained from a Thermo Scientific Nicolet 6700 spectrometer engaging the ATR method with the diamond crystal (4000–400 cm^{-1}, resolution 2 cm^{-1}, 64 scans). PL measurements were performed on photoluminescence (PL) spectrophotometer FLS920, Edinburgh Instruments (Xe lamp with a double monochromator used for excitation in continuous wave regime) at room temperature. The phosphorescence studies were carried out on a self made setup. A laboratory UV lamp (UVLMS-38, Analytik Jena US) operated in the 302 nm mode was used as a light source. An optical guide was used to collect the emitted light from the self-matrix RTP CDs. An Avantes AvaSpec 2048 spectrometer (Avantes B.V., The Netherlands) was used as a detector. The luminance of the self-standing self-matrix RTP CD films was obtained using Chromameter CS 160 (Konica Minolta, Japan). The DRUV/Vis measurement was carried out on a UV–vis spectrometer Avantes Avaspec 2048 with an integration sphere with a 50 mm diameter and an integration time of detector 1000 ms. The reflectance data was converted using the Kubelka Munk function. For the X-ray photoelectron spectroscopy (XPS) measurement, a Kratos Axis Supra spectrometer equipped with a monochromatic X-ray source with Al Kα excitation was used. The binding energy for C1s at 284.8 eV was used as the typical value. Elemental analysis was performed using two methods – ICP and CHNS. Boron content was determined by ICP-OES spectroscopy performed on an iCAP PRO XPS Duo spectrometer (Thermo Scientific) with the use of a boron spectral line at wavelength 249,773 nm. The experimental parameters were set as follows: radial view, 12 mm height, RF power 1050 W, nebulizer gas flow 0,55 l min^{-1}. The CHNS analysis was obtained on Flash 2000 CHNS/O+MAS200R (Thermo Scientific). Two samples were taken from different batches of the prepared material. The amount of 2–3 mg of sample was used, and each analysis was done in triplicate.

Synthesis of Self-Matrix RTP CDs: After careful optimization of the synthesis procedure, ultralong self-matrix RTP CDs were prepared using the well-known heating Method.[6,27] For optimization, two factors, boric acid amount and time period were kept constant and the amount of 1,10

Phenanthroline (10, 20, 50, and 100 mg) was varied to attain maximum RTP. Different temperature conditions (180, 200, 220, and 240 °C) were also optimized to obtain the enhanced RTP. In brief, 3 g of Boric acid and 10 mg of 1,10 phenanthroline were taken in a beaker. To this mixture, 40 mL of distilled water was added and the mixture was covered with a foil (to prevent fast evaporation of water). Then the solution was heated at 200 °C for 5 hrs. After the reaction was complete, the mixture was allowed to cool down overnight at room temperature. The next day, the glassy product was obtained. The product was ground with a mortar and pestle to be used for further characterization and applications. The amount of product obtained after synthesis was ≈1.72 g. The RTP CDs were not exposed to dialysis to prevent the quenching of phosphorescence in aqueous media.

Self-Matrix RTP CDs for Display of Fingerprint: The fingerprint used in the work was obtained from an adult volunteer with his/her consent. The person washed his/her hands and dried them completely. After drying, the person ran his/her thumb finger across her forehead a few times. Then, the thumb finger was placed on a clean glass slide for a few seconds. The ultralong self-matrix RTP CDs were carefully spread on the surface of the glass slide, and the extras were removed using a hair squirrel brush. The glass slide was excited by 302 nm UV excitation light and then switched off. The images were recorded using a mobile phone camera.

The pseudo-anonymized fingerprint in Figure 7b was obtained from a volunteer who gave explicit consent for participation in this research and for the publication of this biometric data. The procedure was approved by the Ethics Committee of the Tomas Bata University on 5. 2. 2024, Reference Number: UTB/24/0 02435.

Self-Matrix RTP CDs for Data Encryption Ink: For the preparation of the security ink, self-matrix RTP CDs were dispersed in water with a concentration of 50 mg mL^{-1}. As a counter-fake ink, the salicylic acid solution was used with ethanol as the solvent.

Preparation of Self-Matrix RTP CDs as a LED Phosphor Material: For the use of self-matrix RTP CDs as a phosphor layer in LEDs, self-matrix RTP CDs were made into pellets. The mold was filled with 80 g of self-matrix RTP CDs, and thin pellets measuring 0.44 mm thick were formed. The pellets were loaded onto the LEDs of wavelength 310 and 340 nm and their corresponding electroluminescence was studied.

Supporting Information

Supporting Information is available from the Wiley Online Library or from the author.

Acknowledgements

The authors are happy to acknowledge the support given by the Ministerstvo Školství, Mládeže a Tělovýchovy for following projects: RP/CPS/2024-28/007, RP/CPS/2024-28/002, RP/CPS/2022/007, and LM2018110. The Internal Grant Agency of Tomas Bata University in Zlin, Czech Republic (IGA/CPS/2023/006 and IGA/CPS/2024/002). The authors are delighted to acknowledge Petr Machac for his help in XPS measurements. Czech-NanoLab project LM2018110 funded by MEYS CR is gratefully acknowledged for the financial support of the XPS measurements at CEITEC Nano Research Infrastructure.

Open access publishing facilitated by Univerzita Tomase Bati ve Zline, as part of the Wiley - CzechELib agreement.

Conflict of Interest

The authors declare no conflict of interest

Data Availability Statement

The data that support the findings of this study are available from the corresponding author upon reasonable request.

Keywords

carbon dots, room temperature phosphorescence, self-matrix, ultralong

Received: March 18, 2024
Revised: June 19, 2024
Published online: July 8, 2024

[1] S. Zhou, F. Wang, N. Feng, A. Xu, X. Sun, J. Zhou, H. Li, *Small* **2023**, *19*, 2301240.
[2] Y. Han, M. Li, J. Lai, W. Li, Y. Liu, L. Yin, L. Yang, X. Xue, R. Vajtai, P. M. Ajayan, L. Wang, *ACS Sustain. Chem. Eng.* **2019**, *7*, 19918.
[3] C. Hao, Y. Bai, L. Zhao, Y. Bao, J. Bian, H. Xu, T. Zhou, F. Feng, *Dyes Pigm.* **2022**, *198*, 109955.
[4] C. Xia, S. Zhu, S.-T. Zhang, Q. Zeng, S. Tao, X. Tian, Y. Li, B. Yang, *ACS Appl. Mater. Interfaces* **2020**, *12*, 38593.
[5] J. Qu, X. Zhang, S. Zhang, Z. Wang, Y. Yu, H. Ding, Z. Tang, X. Heng, R. Wang, S. Jing, *Nanoscale Adv.* **2021**, *3*, 5053.
[6] Q. Feng, Z. Xie, M. Zheng, *Chem. Eng. J.* **2021**, *420*, 127647.
[7] C. Lin, Y. Zhuang, W. Li, T.-L. Zhou, R.-J. Xie, *Nanoscale* **2019**, *11*, 6584.
[8] Y. Zhu, Z. Feng, Z. Yan, X. Yang, *Sens. Actuators, B* **2022**, *371*, 132529.
[9] J. Yang, M. Fang, Z. Li, *Acc. Mater. Res.* **2021**, *2*, 644.
[10] W. Zhao, Z. He, B. Z. Tang, *Nat. Rev. Mater.* **2020**, *5*, 869.
[11] Z. Chen, K. Y. Zhang, X. Tong, Y. Liu, C. Hu, S. Liu, Q. Yu, Q. Zhao, W. Huang, *Adv. Funct. Mater.* **2016**, *26*, 4386.
[12] Z. Yang, Z. Fu, H. Liu, M. Wu, N. Li, K. Wang, S.-T. Zhang, B. Zou, B. Yang, *Chem. Sci.* **2023**, *14*, 2640.
[13] B. Lei, Y. Liu, J. Zhang, J. Meng, S. Man, S. Tan, *J. Alloys Compd.* **2010**, *495*, 247.
[14] W. He, X. Sun, X. Cao, *ACS Sustain. Chem. Eng.* **2021**, *9*, 4477.
[15] X. Wei, J. Yang, L. Hu, Y. Cao, J. Lai, F. Cao, J. Gu, X. Cao, *J. Mater. Chem. C* **2021**, *9*, 4425.
[16] X. Xu, R. Ray, Y. Gu, H. J. Ploehn, L. Gearheart, K. Raker, W. A. Scrivens, *J. Am. Chem. Soc.* **2004**, *126*, 12736.
[17] C. Peng, X. Chen, M. Chen, S. Lu, Y. Wang, S. Wu, X. Liu, W. Huang, *Research* **2021**, *2021*, 6098925.
[18] P. He, Y. Zhu, J. Bai, F. Qin, X. Wang, S. Wu, X. Yu, L. Ren, *J. Lumin.* **2023**, *253*, 119454.
[19] B. Wang, Y. Yu, H. Zhang, Y. Xuan, G. Chen, W. Ma, J. Li, J. Yu, *Angew. Chem., Int. Ed.* **2019**, *58*, 18443.
[20] B. Wang, Z. Sun, J. Yu, G. I. N. Waterhouse, S. Lu, B. Yang, *SmartMat* **2022**, *3*, 337.
[21] H.-y. Wang, L. Zhou, H.-m. Yu, X.-d. Tang, C. Xing, G. Nie, H. Akafzade, S.-y. Wang, W. Chen, *Adv. Opt. Mater.* **2022**, *10*, 2200678.
[22] Y. Wu, E. Xue, B. Tian, K. Zheng, J. Liang, W. Wu, *Nanoscale* **2022**, *14*, 7137.
[23] J. He, Y. Chen, Y. He, X. Xu, B. Lei, H. Zhang, J. Zhuang, C. Hu, Y. Liu, *Small* **2020**, *16*, 2005228.
[24] M. Zan, S. An, M. Jia, L. Cao, L. Li, M. Ge, Z. Wu, Q. Mei, W.-F. Dong, *Microchem. J.* **2022**, *172*, 106878.
[25] W. Li, W. Zhou, Z. Zhou, H. Zhang, X. Zhang, J. Zhuang, Y. Liu, B. Lei, C. Hu, *Angew. Chem., Int. Ed.* **2019**, *58*, 7278.
[26] M. Cheng, L. Cao, H. Guo, W. Dong, L. Li, *Sensors* **2022**, *22*, 2944.
[27] Z. Wang, J. Shen, B. Xu, Q. Jiang, S. Ming, L. Yan, Z. Gao, X. Wang, C. Zhu, X. Meng, *Adv. Opt. Mater.* **2021**, *9*, 2100421.
[28] Z. Zhang, Y.-e. Shi, Y. Liu, Y. Xing, D. Yi, Z. Wang, D. Yan, *Chem. Eng. J.* **2022**, *442*, 136179.
[29] D. Wang, Z. Lu, X. Qin, Z. Zhang, Y.-e. Shi, J. W. Y. Lam, Z. Wang, B. Z. Tang, *Adv. Opt. Mater.* **2022**, *10*, 2200629.
[30] G. Kaur, S. Kainth, R. Kumar, P. Sharma, O. P. Pandey, *React. Kinet., Mech. Catal.* **2021**, *134*, 347.

[31] S. Aghili, M. Panjepour, M. Meratian, *J. Therm. Anal. Calorim.* **2018**, *131*, 2443.
[32] S. Kocakuşak, H. J. Köroğlu, R. Tolun, *Chem. Eng. Proces.: Proc. Intensificat.* **1998**, *37*, 197.
[33] J. Zhang, L.-X. Wang, L. Zhang, Y. Chen, Q.-T. Zhang, *Rare Met.* **2013**, *32*, 599.
[34] S. Mondal, A. K. Banthia, *J. Eur. Ceram. Soc.* **2005**, *25*, 287.
[35] T. L. Nguyen, A. Gascón Nicolás, T. Edvinsson, J. Meng, K. Zheng, M. Abdellah, J. Sá, *Nanomaterials* **2020**, *10*, 1378.
[36] T. Li, C. Wu, M. Yang, B. Li, X. Yan, X. Zhu, H. Yu, M. Hu, J. Yang, *Langmuir* **2022**, *38*, 2287.
[37] Y. Wada, Y. K. Yap, M. Yoshimura, Y. Mori, T. Sasaki, *Diamond Relat. Mater.* **2000**, *9*, 620.
[38] A. Pal, K. Ahmad, D. Dutta, A. Chattopadhyay, *ChemPhysChem* **2019**, *20*, 1018.
[39] P. Shen, Y. Xia, *Anal. Chem.* **2014**, *86*, 5323.
[40] A. I. Large, S. Wahl, S. Abate, I. da Silva, J. J. Delgado Jaen, N. Pinna, G. Held, R. Arrigo, *Catalysts* **2020**, *10*, 1289.
[41] L. Shi, D. Chang, G. Zhang, C. Zhang, Y. Zhang, C. Dong, L. Chu, S. Shuang, *RSC Adv.* **2019**, *9*, 41361.
[42] B. Tian, T. Fu, Y. Wan, Y. Ma, Y. Wang, Z. Feng, Z. Jiang, *J. Nanobiotechnol.* **2021**, *19*, 456.
[43] F. Zhao, T. Zhang, Q. Liu, C. Lü, *Sens. Actuators, B* **2020**, *304*, 127344.
[44] Y. Nie, W. Lai, N. Zheng, W. Weng, *Talanta* **2021**, *233*, 122541.
[45] G. Accorsi, A. Listorti, K. Yoosaf, N. Armaroli, *Chem. Soc. Rev.* **2009**, *38*, 1690.
[46] Y. Wang, J. Yang, Y. Tian, M. Fang, Q. Liao, L. Wang, W. Hu, B. Z. Tang, Z. Li, *Chem. Sci.* **2020**, *11*, 833.
[47] X. Zhang, L. Du, W. Zhao, Z. Zhao, Y. Xiong, X. He, P. F. Gao, P. Alam, C. Wang, Z. Li, J. Leng, J. Liu, C. Zhou, J. W. Y. Lam, D. L. Phillips, G. Zhang, B. Z. Tang, *Nat. Commun.* **2019**, *10*, 5161.
[48] Z. Gan, H. Xu, Y. Hao, *Nanoscale* **2016**, *8*, 7794.
[49] Y.-M. Long, C.-H. Zhou, Z.-L. Zhang, Z.-Q. Tian, L. Bao, Y. Lin, D.-W. Pang, *J. Mater. Chem.* **2012**, *22*, 5917.
[50] B. Wang, S. Lu, *Matter* **2022**, *5*, 110.
[51] Y. Cheng, W. Fan, L. Wang, Y. Liu, S. Yang, Y. Shi, S. Liu, L. Zheng, Q. Cao, *J. Mater. Chem. C* **2022**, *10*, 8806.
[52] M. Park, H. S. Kim, H. Yoon, J. Kim, S. Lee, S. Yoo, S. Jeon, *Adv. Mater.* **2020**, *32*, 2000936.
[53] Q. Li, Y. Li, S. Meng, J. Yang, Y. Qin, J. Tan, S. Qu, *J. Mater. Chem. C* **2021**, *9*, 6796.
[54] L. Ding, X. Jin, Y. Gao, J. Wu, T. Ai, H. Zhou, X. Chen, X. Zhang, W. Chen, *Adv. Opt. Mater.* **2023**, *11*, 2202349.
[55] S. Han, G. Lian, X. Zeng, Z. Cao, Q. Wang, D. Cui, C.-P. Wong, *Nano Res.* **2020**, *13*, 3261.
[56] Y. Sun, J. Liu, X. Pang, X. Zhang, J. Zhuang, H. Zhang, C. Hu, M. Zheng, B. Lei, Y. Liu, *J. Mater. Chem. C* **2020**, *8*, 5744.
[57] Q. Feng, Z. Xie, M. Zheng, *Sens. Actuators, B* **2022**, *351*, 130976.